analytical chemistry

Article

Cite This: Anal. Chem. 2019, 91, 13780−13786

pubs.acs.org/ac

Wavelength-Dependent Surface Plasmon Coupling Electrochemiluminescence Biosensor Based on Sulfur-Doped Carbon Nitride Quantum Dots for K-RAS Gene Detection

Qian Zhang, Yuying Liu, Yixin Nie, Yang Liu, and Qiang Ma*

Department of Analytical Chemistry, College of Chemistry, Jilin University, Changchun, 130012, China

Supporting Information

ABSTRACT: Although graphite phase carbon nitride quantum dots (GCN QDs) showed some advantages in the electrochemiluminescence (ECL) analytical research, the low ECL efficiency limited the potential sensing application. Herein, we synthesized sulfur-doped graphite phase carbon nitride quantum dots (S-GCN QDs) to fabricate a sandwich sensor based on amplified surface plasmon coupling ECL (SPC-ECL) mode. Sulfur doping can change the surface states of QDs effectively and produced new element vacancy. As a result, the ECL efficiency of S-GCN QDs was 2.5× over GCN QDs. Furthermore, compared with the big gap between the ECL peak of GCN QDs (620 nm) and the absorption peak of Au NPs, the doped sulfur elements in S-GCN QDs generated new ECL emission peaks at 555 nm, which was closed to the absorption peak of Au NPs at 530 nm. Due to the wavelength-dependent surface plasmon coupling effect, the ECL peak of S-GCN QDs at 555 nm had greater amplitude of enhancement in the sensing system. The proposed biosensor can quantify the K-RAS gene from 50 fM to 1 nM with a limit of detection (LOD) of 16 fM. We were the first to provide insight into the role of wavelength-dependent surface plasmon coupling in enhancing the sensitivity of ECL biosensor.

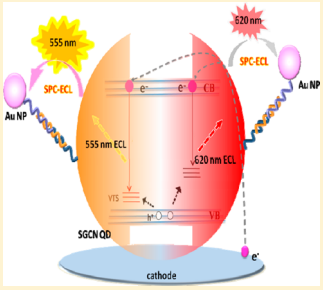

Electrochemiluminescence (ECL) sensing methods has been attracting many scientific research concerns in the biosensing and medical diagnosis application. There were several advantages in the ECL sensing system, including high sensitivity, simplified optical setup, wide detection range, and low background noise. Recently, the graphite-like nanosheets with unique ECL properties have been reported.[1−3] There are several advantages for using nanosheet as ECL sensing material, including stable s-triazine ring structure, high stability and biocompatibility,[1] easy functionalization,[4] and excellent film-forming ability with strong ECL activity.[5] But the large size, low ECL efficiency and poor dispersion of these carbon-based nanosheets limited its further research. In order to overcome the limitation of those nanosheets, the investigation of graphite-like QDs (e.g., graphite QDs and carbon nitride QDs) with an ideal nanostructure and optical properties as a novel luminophor in the ECL sensing system was undertaken.

There were two modified strategies in the improvement of nanoparticle-based ECL sensing ability, including inside-out and outside-in pathway. In the first type, the definite improvement of ECL properties was depend on the optimized structure or changed composition of nanoluminophor. The doping and hybridization with noble metals or rare earth elements in the nanostructure can product remarkable ECL efficiency.[6,7] For example, our group had employed heteroatom dopants to regulate the band gap of boron nitride (BN) QDs. The doped BN QDs can show significant different electro-optical activity and ECL properties. In the second way, the ECL properties of luminophor remained fixed. The ECL signals are amplified in the sensing process via catalytic reaction, self-enhanced ECL reagent, and surface plasmon coupling ECL.[8−10] For example, Wang et al. combined Co^{2+}-based metal organic frameworks and luminol-capped Ag nanoparticles to enhance ECL efficiency.[11] Yuan's group used hollow porous polymeric nanospheres as a self-enhanced ECL reagent to decrease the inner filter effect and minimize inactive emitters and significantly improve the ECL efficiency of ruthenium complex.[12] Our group also established QDs-based ECL biosensor combined ECL resonance energy transfer and surface plasmon coupling ECL (SPC-ECL) sensing mode.[13] In the SPC-ECL mode, the ECL intensity of QDs can be enhanced due to the surface plasmon coupling effect of Au NPs. Among these sensing modes, SPC-ECL was a unique signal enhanced sensing system. It was an important pathway for the weak ECL signal magnification. But the poor spectral overlap between the ECL emission of most carbon-based QDs and the absorption band of Au NPs resulted in the low SPC-ECL sensing working ability. It is necessary to develop wavelength-dependent SPC-ECL. The intensity of enhanced ECL signal strongly depends on the proximity of ECL emission peak of luminophor and plasma absorption peak of precious metal. Therefore, the sensor model based on the above principles is called wavelength-dependent SPC-ECL. Until now, there was an obvious lack of the exploration of wavelength-dependent SPC-ECL research.

Herein, we synthesized sulfur-doped graphite phase carbon nitride QDs (S-GCN QDs) as a new kind of ECL luminophor. Sulfur doping produced element vacancy in GCN QDs and

Received: July 15, 2019
Accepted: October 8, 2019
Published: October 8, 2019

DOI: 10.1021/acs.analchem.9b03212
Anal. Chem. 2019, 91, 13780−13786

Scheme 1. (A) Schematic Illustration of Wavelength-Dependent SPC-ECL Sensor; (B) ECL Mechanism of S-GCN QDs[a]

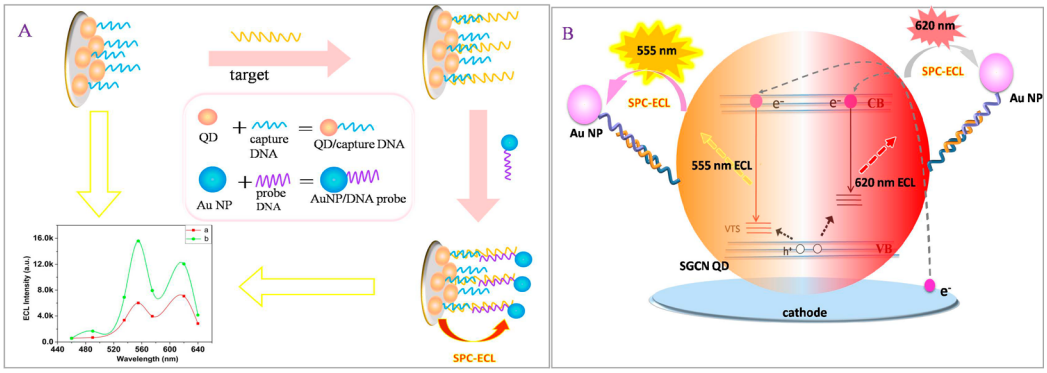

[a]Red and black lines represent ECL radiation paths at 555 and 620 nm, respectively.

made the surface state of S-GCN QDs different from that of pure GCN QDs. The element vacancy was one of internal structural defects, which were highly correlated with controlling and producing a large range of electronic[14−16] and optical properties.[17,18] As a result, the ECL efficiency of S-GCN QDs was boost increased from 0.22% to 0.56% ($[Ru(bpy)_3]^{2+}$ in 0.1 M $K_2S_2O_8$ as a standard, Φ_{st} = 1).[19] Furthermore, the new ECL peak was generated at 555 nm. According to the spectral overlap principle of wavelength-dependent SPC-ECL, the ECL intensity of S-GCN QDs at 555 nm can be increased greatly. At last, S-GCN QDs and the wavelength-dependent SPC-ECL mode combined to construct a biosensor for K-RAS gene detection. The K-RAS gene was an important member of the RAS family. As an upstream gene, its mutation usually implied early form of cancer or adenoma. The mutation rate of the K-RAS gene in pancreatic cancer was up to 70∼100%.[20] Hence, the K-RAS mutation, which is an important biomarker for the early diagnosis of cancers, provides an efficient gene therapy and guidance for the development of specific anticancer drugs.[21,22] The ultrasensitive detection gene is successfully realized based on the S-GCN QD-based SPC-ECL sensing system. As far as we know, it is first reported about the element vacancy-regulated QD electro-optic performance in the wavelength-dependent SPC-ECL sensing research.

EXPERIMENTAL SECTION

Synthesis of S-GCN QDs and GCN QDs. The process was according to the previously reported procedure with a little modification.[3] Citric acid (0.1 g, 0.475 mmol) and thiourea (0.0145 g, 1.9 mmol) were ground into a uniform powder and put into 10 mL of water and put into the microwave (700W) for 40 min at 120 °C. When the reaction finished, the microwave was naturally cooled to ambient temperature. The obtained colorless transparent solution was filtered under stirring for 2 h before use. Five species of S-GCNQDs were synthesized by varying the molar ratio of citric acid to thiourea from 1:1 to 1:2, 1:3, 1:4, and 1:5. Citric acid (0.1 g) was reacted with thiourea (0.0362, 0.0724, 0.109, 0.145, and 0.181 g, respectively). For comparison, we also prepared the GCN QDs with urea and citric acid as precursors under the same conditions. Briefly, 0.101 g urea and 0.081 g citric acid were dissolved in 10 mL of water and put into the microwave (700W) for 40 min at 120 °C. The product was filtered and preserved in a 4 °C refrigerator.

Synthesis of S-GCN QD/Capture DNA and Au NP/DNA Probe. The steps of the synthesis of S-GCN QD/capture DNA were as follows: first, 100 μL of 20 mg/mL EDC and 10 mg/mL NHS were added into 1 mL of S-GCN QDs and the activated carboxyl of S-GCN QDs for 0.5 h. Then, 100 μL of 10 μM capture DNA was injected into the above solutions and reacted for 2 h to form S-GCN QD/capture DNA. In order to remove the unreacted capture DNA, the above solution was filtered through a dialysis membrane (1 kDa) for another 4 h under stirring. Au NPs were prepared by the citrate reduction of $HAuCl_4{\cdot}4H_2O$. The synthesized Au NPs (19 nm) were characterized by TEM (Figure S1). The results revealed that well-dispersed gold nanoparticles were obtained. The Au NP/DNA probe was prepared according to the following steps. First, 50 μL of 1 mg/mL EDC and 0.5 mg/mL NHS were added into 1 mL of Au NPs and the activated carboxyl of Au NPs for 0.5 h. Then, 100 μL of the 10 μM probe DNA was injected into the above solutions and reacted for 2 h to form a Au NP/DNA probe. Last, for removing unreacted probe DNA, the above solution was filtered through a dialysis membrane (1 kDa) for another 4 h under stirring.

Fabrication of ECL DNA Sensor. Scheme 1A outlines the fabricating steps of the ECL DNA sensor. A glassy carbon electrode (GCE) was polished carefully with of 0.3 and 0.05 μm alumina pastes and cleaned thoroughly in an ultrasonic cleaner with alcohol and water sequentially. In order to better fix S-GCN QDs, the electrode was soaked in 0.5 wt % phthalic diglycol diacrylate (PDDA) aqueous solution for 5 min. After drying with N_2, 6 μL of S-GCN QD/capture DNA solution was dropped on the above GCE and blocked with 20 μL of 2 wt % bovine serum albumin (BSA) solution at 37 °C. After drying in the air, then the above working electrode was incubed with 200 μL of different concentrations of target DNA for 6 min at 66 °C and cooled to ambient temperature. Then, 0.01 M Tris-HCl buffers (pH 7.4) washed the electrode extensively to free excess target DNA. Afterward, the above electrode was incubated with 200 μL Au NP/DNA probe for 6 min at 66 °C and cooled to room temperature. When the hybridization was accomplished, 0.01 M Tris-HCl buffers (pH 7.4) washed the electrode extensively to free excess reactions again.

Analysis Procedure. ECL signals were also detected in human serum according to the above procedure. Human serum was got from the third hospital of Jilin university. The serum samples were diluted 50× with ultrapure water and prepared the spiked samples by adding various concentrations of target DNA for use. ECL measurements were performed at ambient temperature and the potential was employed from −2 to 0 V in 0.01 M phosphate buffered saline (PBS, PH 7.4 containing 0.1 M KCl) containing 0.1 M $K_2S_2O_8$.

DOI: 10.1021/acs.analchem.9b03212
Anal. Chem. 2019, 91, 13780−13786

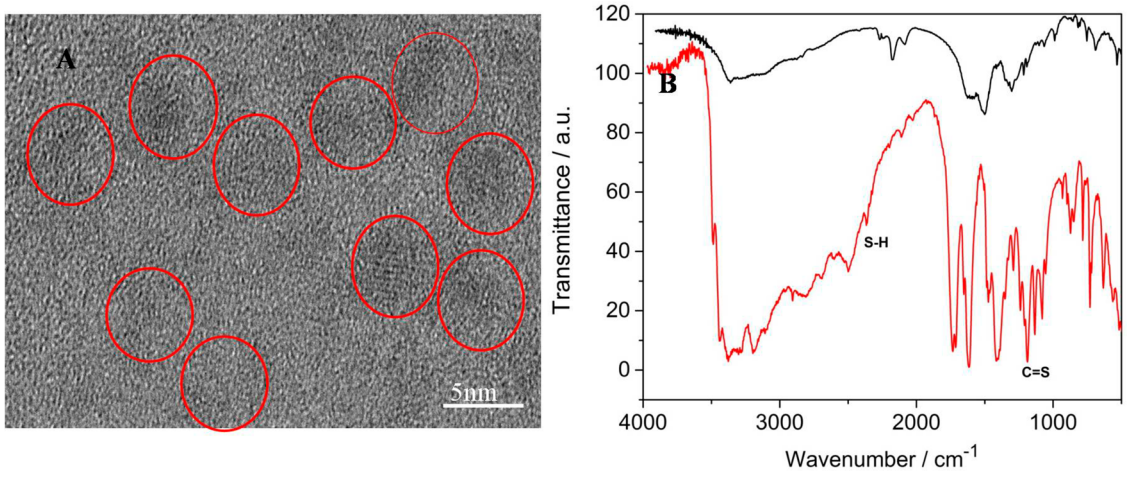

Figure 1. (A) TEM image of S-GCN QDs and (B) FT-IR spectrum of S-GCN QDs (red line) and GCN QDs (black line).

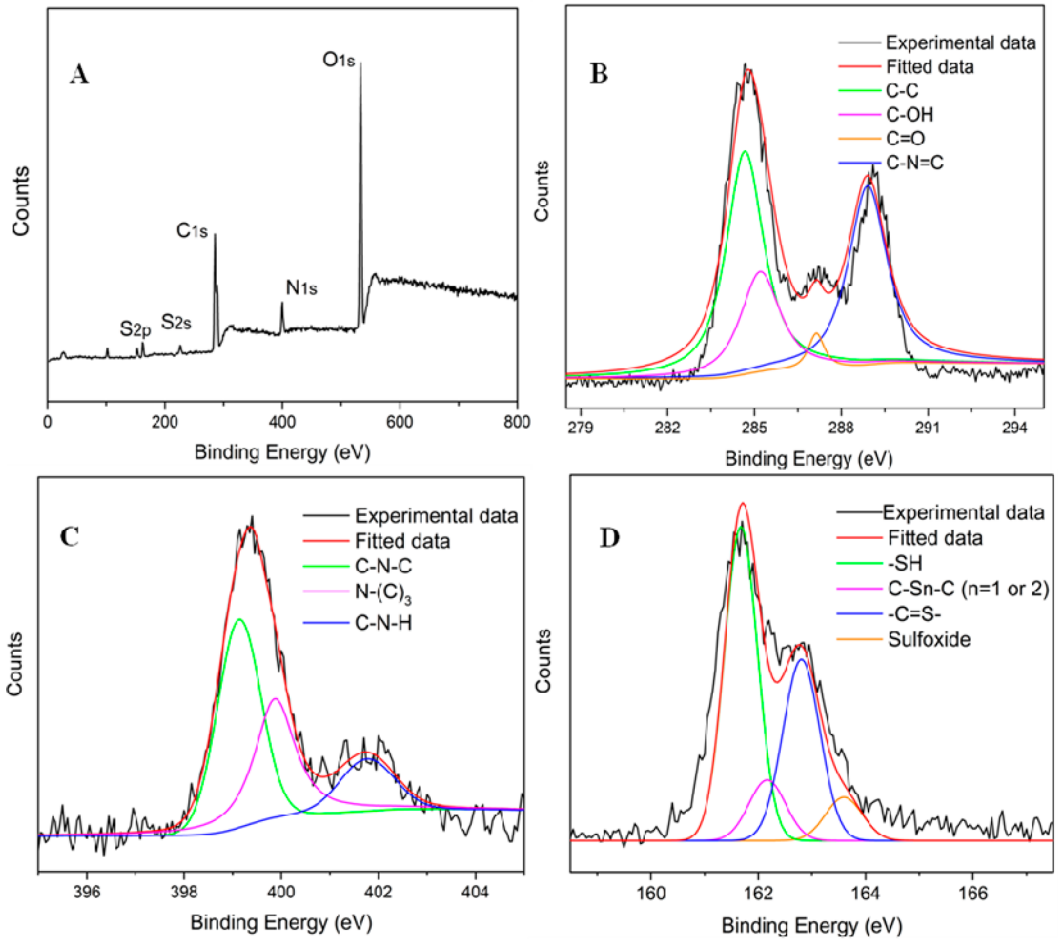

Figure 2. (A) XPS survey spectrum of the S-GCN QDs, and the high-resolution XPS spectra of (B) C_{1S}, (C) N_{1s}, and (D) S_{2p}.

RESULTS AND DISCUSSION

Characterization of S-GCN QDs. As Figure 1A depicted, S-GCN QDs had a mean size of 3 nm with uniform spheres and single good dispersion. FT-IR spectra provided evidence of support for the successful synthesis of S-GCN QDs. From Figure 1B, it was clearly seen that S-GCN QDs had the basic infrared vibration peaks of pure GCN QDs. For instance, the characteristic absorption broad band at 3100−3500 cm^{-1} was assigned to O−H and N−H groups. The typical absorption peak at 807 cm^{-1} came from triazine ring vibration bonds.[23] The absorption peak at 2060 cm^{-1} was assigned to C═N bonds. Also noteworthy is that S-GCN QDs also had some vibration peaks that pure GCN QDs did not possess. For instance, the peak that emerged at 2366 cm^{-1} resulted from the S−H groups, and the peaks that emerged at 1358 and 1185 cm^{-1} corresponded to the stretching vibration of C═N and C═S, respectively. The existence of these functional groups

DOI: 10.1021/acs.analchem.9b03212
Anal. Chem. 2019, 91, 13780−13786

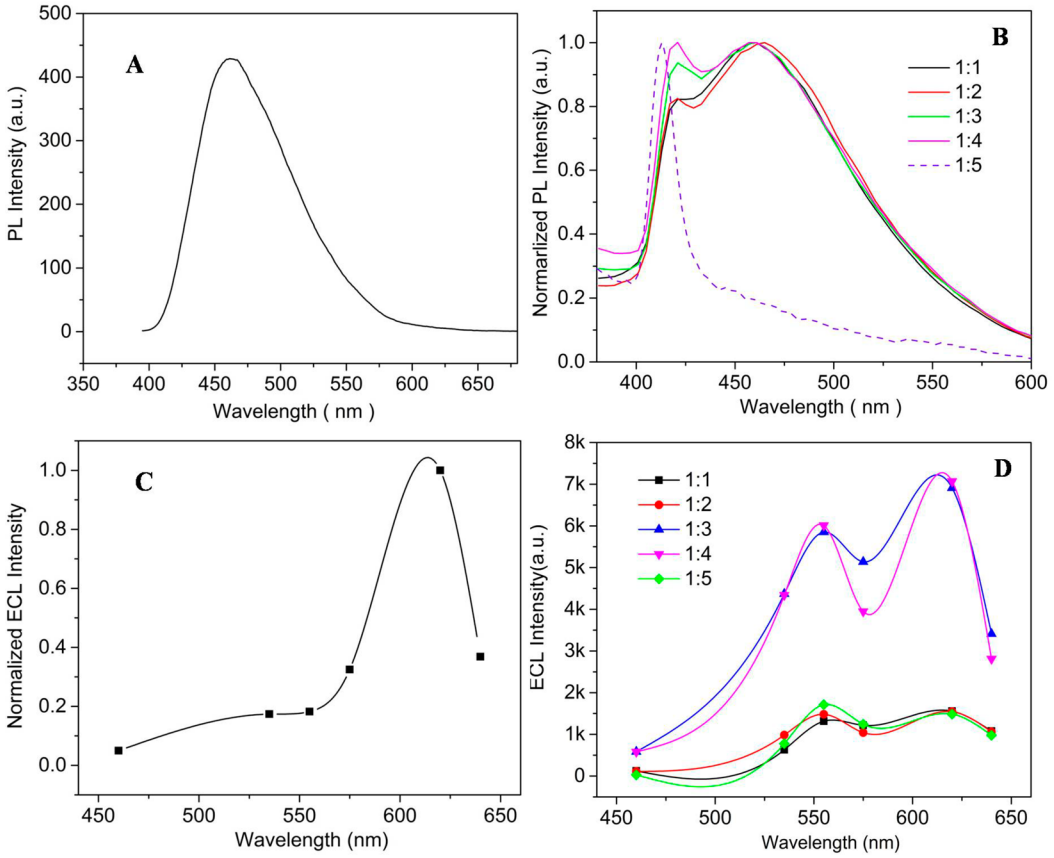

Figure 3. (A) PL spectrum of pure GCN QDs, (B) Normalized PL spectra of the S-GCN QDs synthesized by different proportions of citric acid and thiourea, (C) ECL spectrum of pure GCN QDs, and (D) ECL spectra of S-GCN QDs synthesized by different proportions of citric acid and thiourea.

demonstrated that sulfur was successfully incorporated into GCN QDs.

XPS was used for examining the elements of S-GCN QDs. As is shown in the survey spectrum (Figure 2A), 284.1, 399.1, and 531.9 eV corresponding to three main peaks of O, C, and N elements were detected in S-GCN QDs, respectively. The additional two peaks of S_{2s} and S_{2p} were obseved at 225.2 and 161.7 eV. It indicated that sulfur atoms were indeed introduced into GCN QDs. The high-resolution XPS spectrum of C_{1s} (Figure 2B) revealed the existence of C—OH (285.2 eV), C—N═C (288.9 eV) in the aromatic ring, C—C (284.6 eV) and C═O (287.1 eV).[24,25] As is shown in Figure 2C, three peaks were found in the N_{1s} at 398.4, 400.1. and 401.3 eV, generated by C−N−C, N−$(C)_3$, and C−N−H, respectively. The O_{1S} spectrum was fitted into two peaks (Figure S2) at 532.0 and 533.1 eV, ascribed to C═O and C−OH/C−O−C groups. In addition, the spectrum of S_{2p} (Figure 2D) depicted the peaks at 161.6, 162.2, 163.0, and 163.9 eV, which revealed, respectively, the existence of the −SH, C−S_n−C (n = 1 or 2), sulfoxide, and C═S. These facts confirmed that oxygen- and sulfur-containing groups efficiently functionalized GCN QDs.

PL and ECL Behavior of S-GCN QDs. The optical properties of GCN QDs and S-GCN QDs were characterized by photoluminescence (PL) and ECL spectra. From Figure 3B, under the excitation wavelength of 360 nm, it can be clearly seen that there are two PL emission peaks at 421 and 461 nm in S-GCN QDs. Compared with the pure GCN QDs (Figure 3A), the PL peak at 421 nm was a new emission peak of S-GCN QDs. It indicated that sulfur doping caused the element vacancy and induced new energy level. With the addition of thiourea, the PL emission at 421 nm enhanced from 1:1 to 1:4. When the molar ratio of citric acid (CN precursor) to thiourea (S precursor) was 1:5, there is only one PL peak that appeared at 413 nm. Too much sulfur dopant suppressed GCN QDs intrinsic luminescence at 460 nm. As shown in Figure 3C, there was an ECL emission peak in GCN QDs at 620 nm, which had an obvious red shift compared to the PL emission peak. The ECL spectrum depends strongly on the surface states of GCN QDs. Red-shifted ECL usually occurs when the electrons or holes relax into surface states.[26] A similar phenomenon can also be observed of the other luminophor (e.g., Ge,[27] tetraphenylethylene[28]). In Figure 3D, the ECL emission peak of S-GCN QDs at 620 nm was the same as GCN QDs. Meanwhile, a new ECL peak of S-GCN QDs appeared at 555 nm. It was clear that the ECL intensity of S-GCN QDs synthesized with a ratio of 1:4 citric acid to thiourea was higher than other ratios of QDs. With the addition of sulfur dopant, the active site of S-GCN QDs surface increased. As a result, the ECL signal of S-GCN QDs enhanced with the addition of thiourea from 1:1 to 1:4. When much sulfur dopant (1:5) was added into the GCN QDs structure, the stability of QDs decreased and poor ECL performance was observed. Therefore, S-GCN QDs synthesized with a ratio of 1:4 citric acid to thiourea were selected for subsequent experiments.

The ECL responses of S-GCN QDs were investigated in 0.01 M PBS (pH 7.4) containing 0.1 M $K_2S_2O_8$ (Figure 4A). It can be clearly seen that S-GCN QDs had the higher ECL intensity compared to the undoped GCN QDs. Moreover, with the proportion of S precursor increased, the ECL intensity of S-GCN QDs enhanced, up to nearly three times that of pure GCN QDs. The relation between ECL intensity and S precursor

DOI: 10.1021/acs.analchem.9b03212
Anal. Chem. 2019, 91, 13780−13786

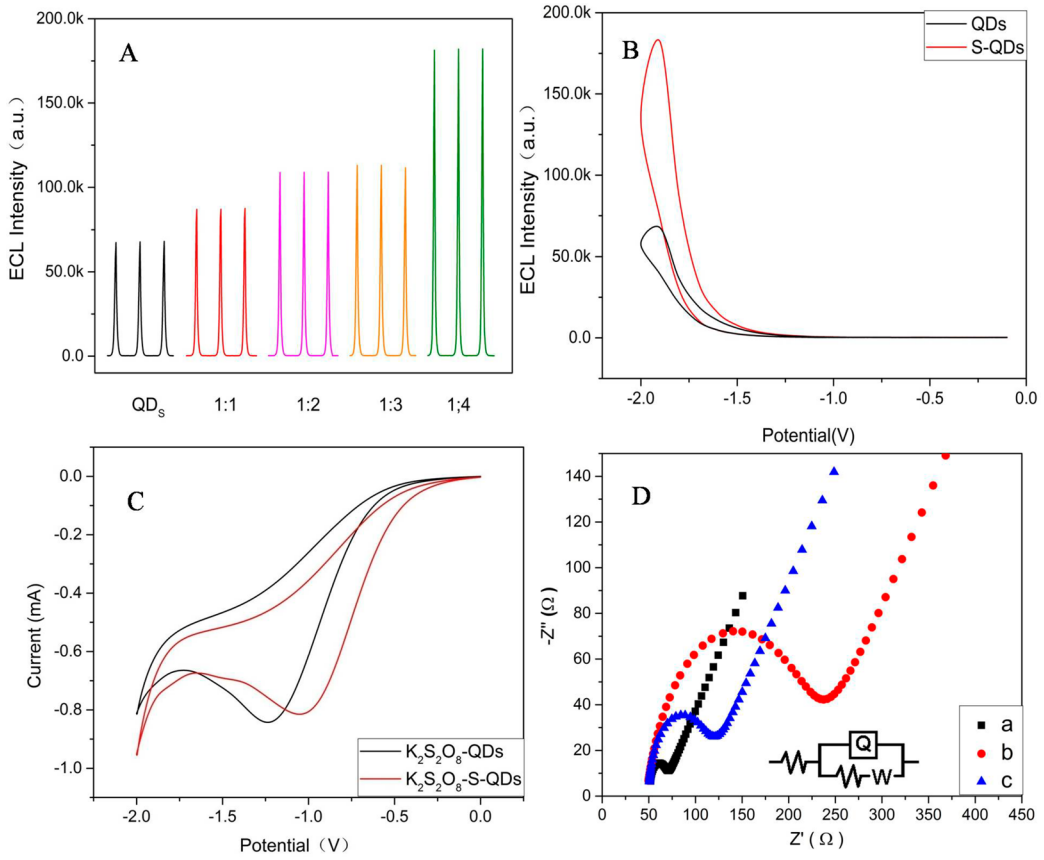

Figure 4. (A) ECL responses of GCN QDs and S-GCN QDs synthesized by different proportions from 1:1 to 1:4. (B) ECL−potential curves of GCN QDs and S-GCN QDs in 0.01 M pH 7.4 PBS containing 0.1 M $K_2S_2O_8$. (C) Cyclic voltammograms (CV) of GCN QD/GCE and S-GCN QD/GCE in 0.1 M pH 7.4 PBS containing 0.1 M $K_2S_2O_8$. (D) EIS of (a) GCE, (b) GCN QD/GE, and (c) S-GCN QD/GE in 0.1 M KCl solution containing 2.5 mM $[Fe(CN)_6]^{3-/4-}$.

proportion was in accordance with the relation of PL intensity. From ECL−potential curves of GCN QDs and S-GCN QDs (Figure 4B), it can be observed that the ECL intensity of S-GCN QDs was three times as much as that of GCN QDs, which can be attributed to sulfur doping induced element vacancy in S-GCN QDs and enhanced the ECL efficiency. The ECL efficiency of S-GCN QDs was 0.56% higher than that of GCN QDs, 0.23% ($[Ru(bpy)_3]^{2+}$ in 0.1 M $K_2S_2O_8$ as a standard, Φ_{st} = 1).[19]

Cyclic voltammograms (CV) of GCN QDs and S-GCN QDs in 0.01 M PBS (pH 7.4) containing 10 mM KCl and 0.1 M $K_2S_2O_8$ were studied and illustrated in Figure 4C. The reduction peak of $K_2S_2O_8$ with GCN QDs was −1.21 V and shifted to −1.03 V with S-GCN QDs. The two reduction peak current were observed come to 0.84 mA and 0.81 mA, respectively. It indicated that the reduction products of S-GCN QDs can react more easily with $K_2S_2O_8$, which was responsible for the generation of strong ECL emission.[29] In Figure 4D, bare GCE had a little semicircle diameter, indicated that the electron transfer impedance (Ret) was little. Compared with GCN QD/GCE (red line, Ret = 177.7 Ω), the Ret clearly decreased for S-GCN QD/GCE (blue line, Ret = 2100 Ω). It demonstrated that the efficiency of electron transfer in S-GCN QDs was faster than GCN QDs, which confirmed that sulfur doping induced active element vacancy.

The ECL mechanism of S-GCN QDs was shown in Scheme 1B. The ECL emission at 620 nm was the same as the radiation mechanism of GCN QDs and other semiconductors.[30] An electron from the cathode injected into the conduction band (CB) of the S-GCN QDs, which formed a negatively charged S-GCN QDs (denoted as S-GCN $QDs^{\bullet-}$, eq 1). At the same time, $S_2O_8^{2-}$ was electro-reduced to strongly oxidizing $SO_4^{\bullet-}$ (eq 2). Then $SO_4^{\bullet-}$ reacted with S-GCN $QDs^{\bullet-}$ to generate excited S-GCN QDs* (eq 3), which subsequently underwent radiation decay to emit light. The possible reaction mechanism was described as follows:

$$\text{S-GCN QDs} + e^- \rightarrow \text{S-GCN QDs}^{\bullet-} \quad (1)$$

$$S_2O_8^{2-} + e^- \rightarrow SO_4^{2-} + SO_4^{\bullet-} \quad (2)$$

$$\text{S-GCN QDs}^{\bullet-} + SO_4^{\bullet-} \rightarrow \text{S-GCN QDs*} + SO_4^{2-} \quad (3)$$

$$\text{S-GCN QDs*} \rightarrow \text{S-GCN QDs} + \hbar\nu \quad (4)$$

The ECL emission at 555 nm was attributed to the element vacancy caused by sulfur doping. The intrinsic vacancy defect can produce an energy trap state (VTS) higher than a valence band (VB) to accept hole.[31] $S_2O_8^{2-}$ was electro-reduced to strongly oxidizing $SO_4^{\bullet-}$ (eq 2), which removed one electron and forms $(\text{S-GCN QDs})_{VTS}^{+\bullet}$ species by introducing a hole at VTS (eq 5). Then, an electron was injected into $(\text{S-GCN QDs})_{VTS}^{+\bullet}$ species, leading to form excited $(\text{S-GCN QDs})_{VTS}$* (eq 6). Lastly, $(\text{S-GCN QDs})_{VTS}$* relaxed and emit ECL emission. The possible reaction mechanism was described as follows:

$$\text{S-GCN QDs} + SO_4^{\bullet-} \rightarrow (\text{S-GCN QDs})_{VTS}^{+\bullet} + SO_4^{2-} \quad (5)$$

DOI: 10.1021/acs.analchem.9b03212
Anal. Chem. 2019, 91, 13780−13786

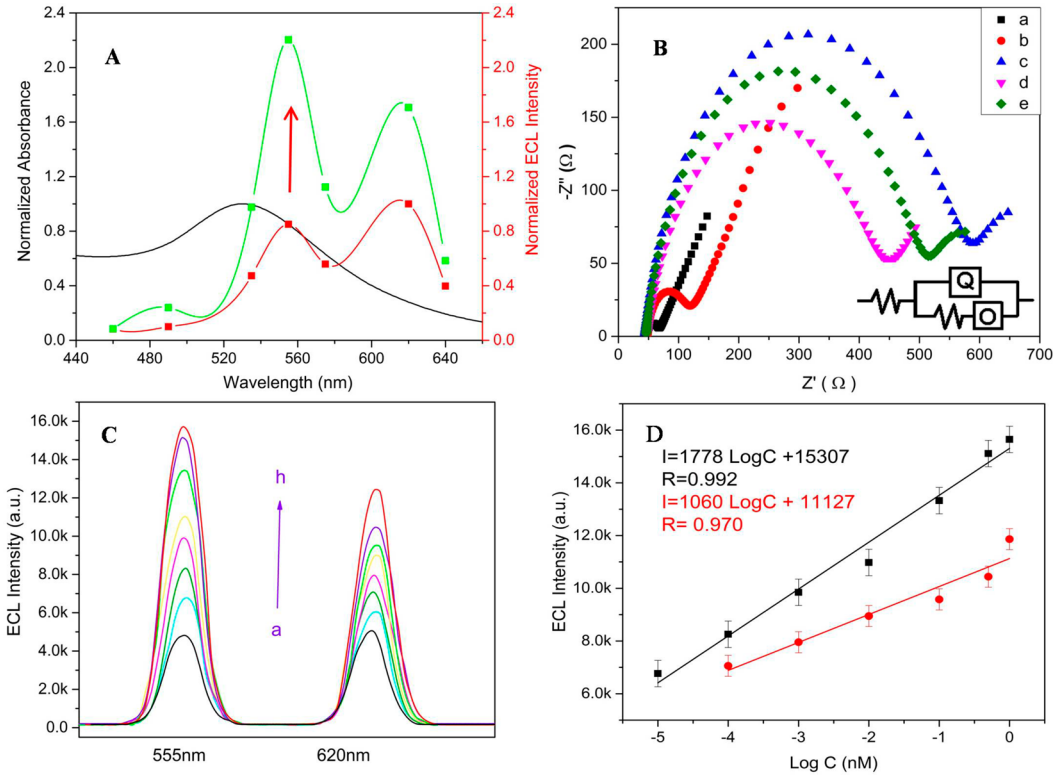

Figure 5. (A) Normalized UV−vis spectrum (black line) of Au NPs and ECL spectra of S-GCN QDs (red line) and Au NP/0.2%CS/S-GCN QD (green line). (B) EIS of (a) GCE, (b) 0.5% PDDA/GCE, (c) S-GCN QD/capture DNA/0.5% PDDA/GCE, (d) target DNA/S-GCN QD/capture DNA/0.5% PDDA/GCE, and (e) Au NP/DNA probe/target DNA/capture DNA/0.5% PDDA/GCE in 0.1 M KCl solution containing 2.5 mM $[Fe(CN)_6]^{3-/4-}$. (C) Relationship between the ECL intensity and different K-RAS gene concentrations (from a to h): blank, 50 fM, 0.1 pM, 1 pM, 0.01 nM, 0.1 nM, 0.5 nM, and 1 nM at 555 and 620 nm. (D) The corresponding calibration plot for K-RAS gene detection.

$$(\text{S-GCN QDs})_{\text{VTS}}^{+\bullet} + e^- \rightarrow (\text{S-GCN QDs})_{\text{VTS}}^* \quad (6)$$

$$(\text{S-GCN QDs})_{\text{VTS}}^* \rightarrow \text{S-GCN QDs} + \hbar\nu \quad (7)$$

Analytical Performance of the Wavelength-Dependent SPC-ECL Biosensor. The UV−vis spectrum (Figure 5A, black line) depicted the surface plasmon absorption peak of Au NPs at about 530 nm. Because the surface plasmon coupling effect strongly dependS on the extent of spectral overlap, the two ECL emission peaks of S-GCN QDs have shown the different change extent. The surface plasmon coupling of Au NPs induced the ECL emission peak at 555 nm greater enhancement (2.6×) than that at 620 nm (1.7×). ECL spectra of GCN QDs and Au NP/0.2%CS/GCN QD were also studied (Figure S3). It is noted that the ECL emission peak of GCN QDs was also enhanced 1.7× due to the SPC of Au NPs. Because the surface plasmon absorption of Au NPs (530 nm) was a broad absorption band, which overlapped a little bit with the ECL emission peak of GCN QDs and S-GCN QDs (620 nm). Consequently, the ECL enhancement was lower than that of S-GCN QDs at 555 nm. EIS was employed to characterize the features of surface-modified electrodes. In Figure 5B, the EIS of bare GCE (curve a) was little. After 0.5% PDDA (curve b) was modified on the bare GCE and Ret increased to 63.33 Ω due to the poor conductivity of PDDA. When S-GCN QDs/capture DNA was connected on the above electrode, there was a distinct increased of Ret to 382.3 Ω. Then, target DNA (curve d) and Au NP/DNA probe (curve e) were immobilized on the modified GCE step by step. Because of the insulating property of DNA, the Ret of each related electrode increased to 419.7 Ω and 522 Ω, respectively. The EIS results demonstrated the successful stepwise fabrication of the ECL DNA sensor.

To evaluate the analytical performance of the constructed biosensor, the ECL DNA sensor was incubated in various concentrations of target K-RAS gene (Figure 5C). With the increase of the concentrations of target DNA incubated, the ECL signals at 555 nm obviously increased more strong than that at 620 nm. As a result, the linear range at 555 nm (50 fM to 1 nM) was broader than that at 620 nm (0.1 pM to 1 nM), and the fitting degree of linear equation is higher (R_{555} = 0.992, R_{620} = 0.970). The detection limit was calculated to 16 fM (LOD = 3σ/S), where σ is the standard deviation of blank signals (n = 3) and S represents the slope of the working plot. We also investigated the analytical performance of the sensor when using the whole ECL emission without wavelength-resolution (Figure S4). The linear range is from 0.1 pM to 1 nM and LOD is 30 fM. Although the whole ECL signal is obviously higher than the wavelength-resolved ECL, the increasing extents of the whole ECL signal reduced. As a result, the analytical performance of the sensor without wavelength-resolved were inferior to that of wavelength-dependent SPC-ECL.

Compared with the other methods for detecting K-RAS gene (Table S2), the wavelength-dependent SPC-ECL biosensor in this work was more sensitive than other reports. It attribute to the perfect surface plasmon coupling between Au NPs and S-GCN QDs. Besides, the selectivity of the wavelength-dependent SPC-ECL biosensor was demonstrated by the interference experiments (Figure S5). It was found that the same concentration of the one-base mismatched DNA did not affect the analytical performance of the wavelength-dependent SPC-

DOI: 10.1021/acs.analchem.9b03212
Anal. Chem. 2019, 91, 13780−13786

ECL biosensor. The biosensor was employed to measure the K-RAS gene in human serum (Table 1). The recoveries of the K-RAS gene were 92.0%−103%, and relative standard deviation (RSD) was below 4.03%. Therefore, the proposed ECL DNA sensor can detect the K-RAS gene in real sample analysis.

Table 1. Determination of Target DNA in Serum Samples

sample	spiked (nM)	founded (nM)	recovery (%)	RSD (%; n = 3)
1	1.0	0. 96	96.0	4.03
2	0.01	0.0103	103.0	3.67
3	0.0001	0.00 98	98.0	2.50

CONCLUSION

In this work, S-GCN QDs were successfully synthesized to construct a wavelength-dependent SPC-ECL biosensor. Sulfur doping produced the element vacancy in S-GCNQDs. The ECL luminescence efficiency increased 2.5 times over GCN QDs. Moreover, there are two emission peaks (555 and 620 nm, respectively) in the ECL spectrum of S-GCN QDs. The ECL emission at 555 nm was attributed to the element vacancy, which has good spectral overlap with the absorption band of Au NPs. As a result, a K-RAS gene sensor based on the SPC-ECL mode was fabricated. The proposed biosensor achieved satisfactory detection results with high sensitivity and selectivity. The wavelength-dependent SPC-ECL sensing mode had great application potential in future analytical research.

ASSOCIATED CONTENT

Supporting Information

The Supporting Information is available free of charge on the ACS Publications website at DOI: 10.1021/acs.analchem.9b03212.

Chemicals and apparatus, ECL efficiency of the QDs, TEM of Au NPs (Figure S1), high-resolution O_{1s} XPS spectra of S-GCN QDs (Figure S2), normalized UV−vis spectrum of Au NPs and ECL spectra of GCN QDs and Au NP/0.2%CS/GCN QD (Figure S3), the analytical performance of the sensor when using the whole ECL emission without wavelength-resolved (Figure S4), comparison of the ECL intensity changes for the sensors hybridized with target DNA, one-base mismatched target DNA (Figure S5), sequences of the used oligonucleotides in present work (Table S1), and the comparison of the various methods for detecting K-RAS gene (Table S2) (PDF)

AUTHOR INFORMATION

Corresponding Author

*Tel.: +86-431-85168352. E-mail: qma@jlu.edu.cn.

ORCID

Qiang Ma: 0000-0003-4841-5005

Notes

The authors declare no competing financial interest.

ACKNOWLEDGMENTS

The present work was supported by the Youth Science Fund of Jilin Province (20140520081JH), the "Thirteenth Five Year" Project of the Science and Technology Research in the Education Department of Jilin Province, China.

REFERENCES

(1) Zhang, X.; Xie, X.; Wang, H.; Zhang, J.; Pan, B.; Xie, Y. *J. Am. Chem. Soc.* **2013**, *135*, 18−21.
(2) Feng, Q. M.; Shen, Y. Z.; Li, M. X.; Zhang, Z. L.; Zhao, W.; Xu, J. J.; Chen, H. Y. *Anal. Chem.* **2016**, *88*, 937−944.
(3) Li, H.; Shao, F.-Q.; Huang, H.; Feng, J.-J.; Wang, A.-J. *Sens. Actuators, B* **2016**, *226*, 506−511.
(4) Chen, L.; Zeng, X.; Si, P.; Chen, Y.; Chi, Y.; Kim, D. H.; Chen, G. *Anal. Chem.* **2014**, *86*, 4188−4195.
(5) Chen, L.; Huang, D.; Ren, S.; Dong, T.; Chi, Y.; Chen, G. *Nanoscale* **2013**, *5*, 225−230.
(6) Du, X.; Jiang, D.; Dai, L.; Zhu, W.; Yang, X.; Hao, N.; Wang, K. *Anal. Chem.* **2018**, *90*, 3615−3620.
(7) Liu, Y.; Wang, M.; Nie, Y.; Zhang, Q.; Ma, Q. *Anal. Chem.* **2019**, *91*, 6250−6258.
(8) Huang, Y.; Li, L.; Zhang, Y.; Zhang, L.; Ge, S.; Yu, J. *Biosens. Bioelectron.* **2019**, *126*, 339−345.
(9) Song, X.; Li, X.; Wei, D.; Feng, R.; Yan, T.; Wang, Y.; Ren, X.; Du, B.; Ma, H.; Wei, Q. *Biosens. Bioelectron.* **2019**, *126*, 222−229.
(10) Li, M. X.; Feng, Q. M.; Zhou, Z.; Zhao, W.; Xu, J. J.; Chen, H. Y. *Anal. Chem.* **2018**, *90*, 1340−1347.
(11) Wang, S.; Zhao, Y.; Wang, M.; Li, H.; Saqib, M.; Ge, C.; Zhang, X.; Jin, Y. *Anal. Chem.* **2019**, *91*, 3048−3054.
(12) Chen, A.; Zhao, M.; Zhuo, Y.; Chai, Y.; Yuan, R. *Anal. Chem.* **2017**, *89*, 9232−9238.
(13) Liu, Y.; Chen, X.; Wang, M.; Ma, Q. *Green Chem.* **2018**, *20*, 5520−5527.
(14) Meng, W.; Saparov, B.; Hong, F.; Wang, J.; Mitzi, D. B.; Yan, Y. *Chem. Mater.* **2016**, *28*, 821−829.
(15) Jung, S. J.; Jeong, T.; Shim, J.; Park, S.; Park, J.-h.; Shin, B. G.; Song, Y. J. *Curr. Appl. Phys.* **2019**, *19*, 224−229.
(16) Zhu, Q.; Chen, W.; Cheng, H.; Lu, Z.; Pan, H. *ChemCatChem* **2019**, *11*, 2667−2675.
(17) He, Y.; Hou, S.; Yang, L.; Zhang, F.; Zou, G. *Chem. - Eur. J.* **2018**, *24*, 9592−9597.
(18) Li, X.; Cheng, Y.; Wu, Q.; Xu, J.; Wang, Y. *Appl. Catal., B* **2019**, *240*, 270−276.
(19) Richter, M. M. *Chem. Rev.* **2004**, *104*, 3003−3036.
(20) Zhou, Z.; Zhu, D.; Xing, D. *Acta Chim. Sinica* **2006**, *12*, 1279−1283.
(21) Li, H.; Tang, Y.; Zhao, W.; Wu, Z.; Wang, S.; Yu, R. *Anal. Chim. Acta* **2019**, *1065*, 98−106.
(22) Rosi, N. L.; Mirkin, C. A. *Chem. Rev.* **2005**, *105*, 1547−1562.
(23) Yin, Y.; Zhang, Y.; Gao, T.; Yao, T.; Han, J.; Han, Z.; Zhang, Z.; Wu, Q.; Song, B. *Mater. Chem. Phys.* **2017**, *194*, 293−301.
(24) Zhou, Z.; Shen, Y.; Li, Y.; Liu, A.; Liu, S.; Zhang, Y. *ACS Nano* **2015**, *9*, 12480−12487.
(25) Liu, C. G.; Wu, X. T.; Li, X. F.; Zhang, X. G. *RSC Adv.* **2014**, *4*, 62492−62498.
(26) Sun, L. F.; Bao, L.; Hyun, B. R.; Bartnik, A.; Zhong, Y. W.; Reed, J.; Pang, D. W.; Abruña, H. D.; Malliaras, G. G.; Wise, F. W. *Nano Lett.* **2009**, *9*, 789−793.
(27) Myung, N.; Lu, X.; Johnston, K. P.; Bard, A. J. *Nano Lett.* **2004**, *4*, 183−185.
(28) Liu, J.-L.; Zhang, J.-Q.; Tang, Z.-L.; Zhuo, Y.; Chai, Y.-Q.; Yuan, R. *Chemical Science* **2019**, *10*, 4497−4501.
(29) Dong, Y. P.; Wang, J.; Peng, Y.; Zhu, J. J. *Biosens. Bioelectron.* **2017**, *89*, 1053−1058.
(30) Cheng, C.; Huang, Y.; Tian, X.; Zheng, B.; Li, Y.; Yuan, H.; Xiao, D.; Xie, S.; Choi, M. M. *Anal. Chem.* **2012**, *84*, 4754−4759.
(31) Wang, F.; Lin, J.; Zhao, T.; Hu, D.; Wu, T.; Liu, Y. *J. Am. Chem. Soc.* **2016**, *138*, 7718−7724.

DOI: 10.1021/acs.analchem.9b03212
Anal. Chem. 2019, 91, 13780−13786